Neurospine 2024;21(3):878-889.
https://doi.org/10.14245/ns.2448546.273

Neurospine
pISSN 2586-6583 eISSN 2586-6591

Original Article

**Corresponding Author**
Hemant Kumar
https://orcid.org/0000-0002-6434-0245

Department of Pharmacology and Toxicology, National Institute of Pharmaceutical Education and Research (NIPER)-Ahmedabad, Gandhinagar, India
Email: hemantbhave@gmail.com, hemant@niperahm.res.in

**Co-corresponding Author**
Amit Shard
https://orcid.org/0000-0003-4109-6275

Department of Medicinal Chemistry, National Institute of Pharmaceutical Education and Research (NIPER)-Ahmedabad, Gandhinagar, India
Email: amit@niperahm.res.in

Received: May 28, 2024
Revised: July 23, 2024
Accepted: July 26, 2024

*Abhishek Roy and Santimoy Sen contributed equally to this study as co-first authors.



# Modulation of the LIMK Pathway by Myricetin: A Protective Strategy Against Neurological Impairments in Spinal Cord Injury

Abhishek Roy[1,*], Santimoy Sen[1,*], Rudradip Das[2], Amit Shard[2], Hemant Kumar[1]

[1]Department of Pharmacology and Toxicology, National Institute of Pharmaceutical Education and Research (NIPER)-Ahmedabad, Gandhinagar, India
[2]Department of Medicinal Chemistry, National Institute of Pharmaceutical Education and Research (NIPER)-Ahmedabad, Gandhinagar, India

**Objective:** Spinal cord injury (SCI), one of the major disabilities concerning central nervous system injury, results in permanent tissue loss and neurological impairment. The existing therapeutic options for SCI are limited and predominantly consist of chemical compounds. In this study, we delved into the neuroprotective effects of myricetin, a natural flavonoid compound, and the underlying mechanisms, specifically in the context of SCI, utilizing an *in vivo* model. Previously, our investigations revealed an elevation in the phosphorylated form of Lin-11, Isl-1, and Mec-3 kinase1 (LIMK1) at chronic time points postinjury, coinciding with neuronal loss and scar formation. Our primary objective here was to assess the potential neuroprotective properties of myricetin in SCI and to ascertain if these effects were linked to LIMK inhibition, a hitherto unexamined pathway to date.
**Methods:** Computational docking and molecular dynamics simulation studies were performed to assess myricetin's potential to bind with LIMK. Then, using a rat contusion model, SCI was induced and different molecular techniques (Western blot, Evans Blue assay, quantitative reverse transcription polymerase chain reaction and immunohistochemistry) were performed to determine the effects of myricetin.
**Results:** Remarkably, computational docking models identified myricetin as having a better interaction profile with LIMK than standard. Subsequent to myricetin treatment, a significant downregulation in phosphorylated LIMK expression was observed at chronic time points. This reduction correlated with a notable decrease in glial and fibrotic scar formation, and enhanced neuroprotection indicating a positive outcome *in vivo*.
**Conclusion:** In summary, our findings underscore myricetin's potential as a bioactive compound capable of attenuating SCI-induced injury cascades by targeting the LIMK pathway.

**Keywords:** Spinal cord injury, LIM kinase, Myricetin, Glial scar, Functional recovery

## INTRODUCTION

Spinal cord injury (SCI) refers to a series of events, including a primary mechanical injury and a cascade of secondary injuries, ultimately leading to a tremendous socioeconomic impact on affected individuals and the healthcare system.[1] The extrinsic restrictive environment and an inherent decay of permissive conditions could be attributed to SCI repair failure.[2] Repulsive axon guidance molecules, myelin-associated inhibitors, and glial scar-associated inhibitors are examples of inhibitors of central nervous system (CNS) regeneration.[3] Interestingly, a large number of these growth inhibitory molecules elicit their effects via means of RhoA-ROCK signaling activation. In turn, RhoA/ROCK activation induces downstream effectors that control cytoskeletal rearrangement, including neurite outgrowth inhibition and growth cone collapse.[4]

In the early stages of neuronal maturation, specific control of neuronal migration, growth cone motility, axon guidance, and neurite outgrowth is essential for the complicated process of neural network development. In these pathways, Rho GTPases and their upstream and downstream effectors are implicated.[5,6] Lin-11, Isl-1, and Mec-3 kinases (LIMKs) are one of such downstream effectors of Rho GTPases expressed in various cell types including neurons. Members of the kinase family LIMK1 and 2 are distinguished by their dual tyrosine kinase and serine/threonine kinase activity.[7] LIMKs are known to influence microtubule dynamics in the interphase cell cycle and to regulate the conversion of filamentous actin (F-actin) into globular actin (G-actin) through the phosphorylation of cofilin substrates.[8] LIMK and other microtubule-associated proteins can improve microtubule stability when in their unphosphorylated or inactive state. Specifically, the effects of LIMK on microtubule dynamics are the result of direct contact between LIMK and tubulin: when LIMK is inactivated, microtubules are stabilized by acetylation or detyrosination, whereas microtubule depolymerization is observed with LIMK overexpression.[9] Rats administered with complete Freund's adjuvant (CFA) injection, which results in inflammatory heat hyperalgesia, exhibited elevated LIMK activity in dorsal root ganglion (DRG) neurons. This was accompanied by phosphorylation and consequent inactivation of the LIMK substrate, cofilin. The heat hyperalgesia exerted by CFA was reduced by interventions that decreased LIMK activity, inhibited cofilin phosphorylation, or disrupted actin filaments in DRG neurons.[10] In our previous study, we showed that an elevated phosphorylation of LIMK leads to glial scar development and neuronal retraction at chronic time points of SCI. Phosphorylation of LIMK was found to be responsible for microtubule instability, which resulted in an obstruction in neuronal development. Improved neuroprotection by microtubule stabilization and mitigation of scar formation was demonstrated to be facilitated by inhibition of LIMK at chronic time periods after SCI, i.e., day post injury 28 (DPI-28).[11]

Flavonoids are an important family of phytochemicals that belong to plant secondary metabolites and have exceptional pharmacological properties like antioxidant, anti-inflammatory, antiaging, and so forth.[12] Myricetin is a such a flavonoid component found in a variety of plants, including vegetables, fruits, berries, tea, and herbal remedies.[13] Studies have demonstrated that myricetin can traverse the blood-brain barrier, exhibiting antioxidative, anti-inflammatory, and antiproliferative activities.[14,15] Myricetin was found to exhibit anti-inflammatory and neuroprotective properties following traumatic brain injury, via managing the epidermal growth factor receptor-protein kinase B (EGFR-AKT)/signal transducer and activator of transcription (STAT) signaling cascade and the phosphorylation states of AKT and STAT1. Through an increased EGFR expression and AKT phosphorylation, which inhibits apoptosis, myricetin increased interleukin (IL)-4 and IL-10 secretion, 2 anti-inflammatory cytokines that limit excessive neuroinflammation after traumatic brain injury.[16] In another research, myricetin improved brain damage and neurological impairments in middle-aged rats through nuclear factor erythroid 2-related factor 2 activation following experimental stroke.[17] Despite advancements, there remains a gap in exploring natural products as LIMK inhibitors to mitigate SCI. Therefore, this study pioneers the investigation into the effects of myricetin on the LIMK pathway, inflammation, neuroprotection, and functional recovery in SCI rats.

## MATERIALS AND METHODS

### 1. Computational Docking Model

The Protein Data Bank (PDB) was utilized to obtain the crystal structure of LIMK (PDB id–7B8W), which was then used to mimic the protein structure in this work. The protein structures were refined in terms of bond order, formal charges, missing hydrogen atoms, topologies, and incomplete and terminal amide groups. Water molecules were removed beyond the heteroatom's 5Å range, and all possible ionization states for each heteroatom in the protein structure were generated, and the most stable state was selected. The retained water molecules' orientations were changed, and the hydrogen bonds were distributed. A restricted reduction of the protein structure was carried out using the OPLS2005 force field to realign side-chain hydroxyl groups and lessen potential steric conflicts. ChemDraw Ultra version 20.0 was used to build the ligand structures in the CDX format, and the LigPrep module of Maestro 12.7.161 was used to execute these ligands in the Schrödinger suite 2023 after being converted to mol2 format. The ligands' charged groups were neutralized, and their bond ordering was filled. The optimized ligands were used for docking investigations, with the receptor grid preserved in its crystal structure. The accuracy of the docking process was evaluated by contrasting an experimental binding mode discovered by x-ray crystallography with the lowest energy pose predicted by the object scoring function, Glide score (G Score). Hydrogen bonding interactions and the root mean square deviation (RMSD) between the predicted and actual x-ray crystallographic conformations were used to analyze the data. The chosen compounds were glide-docked using the receptor grid and already-made ligand molecules. The docking technique was executed in flexible docking mode, which automatically generates conformations for each input ligand. A series of hierarchical fitters were used to evaluate the ligand's interaction with the receptor. The fitness ratings for each ligand in LIMKs were compared together with a summary of the active compounds' XP-Glide scores.[18] To determine the relative LIMK modulation activity, the glide scores of the examined compounds were compared to those of the reference BMS-5, a potent inhibitor of LIMKs.

**2. Molecular Dynamic Simulation Studies**

The stability of the docked myricetin/LIMK complex was evaluated through a 100 ns MD simulation analysis. The complex was examined using Schrödinger 2023's Desmond module in an explicit solvent system with an OPLS3 force field. The molecular system was solvated using crystallographic water molecules under orthorhombic periodic boundary conditions. Na+ was used as counter ions to neutralize the system. An ensemble of Nose-Hoover thermostats and a barostat was used to maintain consistent temperatures and pressures. A hybrid energy minimization method was applied, and the Broyden-Fletcher-Goldfarb-Shanno approach was used to reduce energy. A Smooth Particle Mesh Ewald method was used for long-range electrostatic interactions. Multiple time step reference system propagator algorithm integrations were used for bonded, near-bonded, and far-bonded interactions. Data was collected every 100 picoseconds, and the resulting trajectory was assessed using the Maestro 12.7.161 (Schrödinger, Inc., New York, NY, USA) graphical user interface.[19]

**3. SCI Model Induction**

Female Sprague-Dawley rats of weights ranging from 220–260 g were used to carry out this experimental framework. The animals were procured after they were approved by the Institutional Animal Ethics Committee (IAEC No.: IAEC/021/009). Guidelines and instructions issued by the IAEC were strictly followed after the procurement of animals, including the surgical procedures performed on them, followed by postoperative care and euthanasia. Animals were anaesthetized using a mixture of Ketamine and Xylazine with the dose of 75 mg/kg and 10 mg/kg respectively; intraperitoneally. The incision was made after determining the T10–12 vertebrae following the laminectomy. Spinal cord contusion was performed with impactor (RWD, 68097) by dropping a weight of 10 g from 10-cm height. The muscles and the skin layers were sutured following surgery. The sham group underwent laminectomy without the further processes and was sutured thereafter. Twice daily, gentamicin (i.m.) and buprenorphine (i.p.) were administered for the initial week after surgery. Until the restoration of regular urinary function occurred, the urinary bladder was evacuated twice daily.

**4. Administration of the Compound**

Myricetin (Sigma Aldrich; 70050) 10 mg/kg was administered orally using oral gavage, 1-hour postinjury. The drug was uniformly suspended in 5% ethanol. For vehicle group 5% ethanol solution in saline was administered 1hour post injury. The dosing was continued till 7-day postinjury, once a day, for long-term study animals. For short-term studies (DPI-1), the drug was administered only once, 1-hour postsurgery.

**5. Western Blot Analysis**

Animals were sacrificed, and spinal cord tissue from the injury epicenter was isolated. 30 μg of protein was loaded in each well and were separated by sodium dodecyl sulfate polyacrylamide gel electrophoresis, following which the protein was transferred from the gel to the polyvinylidene fluoride membrane through TransBlot assembly (Bio-Rad). The membranes were blocked with 5% bovine serum albumin for 1 hour at room temperature, following which the membranes were incubated overnight at 4°C in primary antibodies, namely p-LIMK1 (1:750, ab194798, Abcam), KIF5B (1:5,000, ab167429, Abcam), and GAPDH (1:10,000, ab8245, Abcam). The day-after incubation, the membranes were washed thrice with Tris-buffered saline with 0.1% Tween 20 (TBST). This step was followed by incubation in HRP-conjugated secondary antibody (1:10,000, ab6721, Abcam) for 1 hour, after which the membranes were washed again with TBST and visualized using enhanced chemiluminescence solution (Bio-Rad; 170-5061) in which Gel Documentation System (Bio-Rad) was used for detection of protein bands. The densitometric analysis was performed using ImageJ software.

**6. Evans Blue Assay**

To measure the integrity of the blood-spinal cord barrier (BSCB), we performed this assay. Twenty-four hours after SCI, 0.5 mL of 2% Evans blue (Sigma Aldrich) was administered intravenously to rats and sacrificed by transcardial perfusion after 30 minutes of administration of Evans blue. A 2-cm-long spinal cord was isolated with the injury area intact at the center. This


https://doi.org/10.14245/ns.2448546.273

was succeeded by homogenization in a 50% trichloroacetic acid and a 10-minute centrifugation at 10,000 g (ThermoFisher Scientific). A multimode reader was used to detect the spectrophotometric absorbance at 620 nm in the supernatant collected. A standard curve was generated with a predetermined concentration of Evans blue. Based on the standard curve, the concentration of evans blue in the sample was estimated as microgram (μg) of Evans blue per milligram (mg) of tissue.

### 7. Quantitative Real-Time PCR

The rats were sacrificed after 24 hours of injury, and spinal cord tissue was isolated with the injury portion in the centre. Using the NanoDrop method (Thermo Scientific, NanoDrop 2000C), the RNAs were quantified after being extracted with Invitrogen's TRIzol Reagent. This step is followed by cDNA synthesis using a cDNA synthesis kit (Bio-Rad), using a Thermocycler. According to the Bio-Rad Universal SYBR Green protocol, the cDNA samples and the desired primers were diluted and the polymerase chain reaction (PCR) was performed using a quantitative reverse transcription PCR (RT-PCR) machine (Bio-Rad). The RT-PCR was carried out using the following parameters: an initial step at 95°C for 10 minutes, a second phase at 95°C for 15 seconds, and an annealing temperature of 60°C for 30 seconds for 40 cycles with melt curve analysis The data were represented as Ct or cycle threshold values, using 18s as internal control. The primers that were used: IL-6 (Forward Rat 5′-CAGAGTCATTCAGAGCAATAC-3′; Reverse Rat 5′-CTTTCAAGATGAGTTGGATGG-3′), IL-1β (Forward Rat 5′-TAAGCCAACAAGTGGTATTC-3′; Reverse Rat 5′-AGGTATAGATTCTTCCCCTTG-3′), CCL3 (Forward Rat 5′-GTCATTTTCCTGACCAAGAG-3′; Reverse Rat 5′-CCTCTAATCTCAGGCATTTAG-3′).

### 8. Tissue Fixation and Paraffin Block Preparation

At 28th day post-SCI, rats were anaesthetized and transcardial perfusion with 0.9% saline and 4% paraformaldehyde (PFA) was conducted. The spinal cord was then isolated and submerged in 4% PFA (Sigma Aldrich) overnight at 4°C. The spinal cord was immersed for 2 hours each in gradient ethanol (70, 80, 90, and 100%) and xylene. A paraffin embedder machine (ThermoFisher Scientific) was used to make the paraffin blocks of the tissues. The blocks were sliced lengthwise and microtome sections of 5 μm were produced (Leica).

### 9. Immunohistochemistry

After rehydration, pepsin (Sigma Aldrich) was used to extract antigens from the sections, followed by 5 minutes of 3% hydrogen peroxide in methanol to inhibit endogenous peroxidase. The sections were incubated overnight at 4°C with the primary antibody after blocking for 5 minutes with a protein blocker (Abcam). The primary antibodies used were βIII-tubulin (1:500, T2200, Sigma), GFAP (1:500, ab4674, Abcam), Laminin (1:75, L9393, Sigma). Secondary antibodies were Alexa Fluor 647 (1:1,000, ab150079, Abcam), Alexa Fluor 568 (1:1,000, ab175477, Abcam). Alexa Fluor-conjugated secondary antibodies were incubated for one hour at room temperature, away from the light, after a series of phosphate-buffered saline with Tween 20 (PBS-T) washes. Each segment was then stained with DAPI (4′6-diamidino-2-phenylindole) (1:1,000) for 10 minutes to help identify the nuclei. Dibutylphthalate polystyrene xylene was used to mount the sections after they were washed with PBS-T twice more. Slides were examined using confocal microscopy (Leica) at the required laser wavelength to obtain a fluorescence image. The fluorescence intensity was analyzed using ImageJ software.

### 10. Evaluation of Functional Recovery

Evaluation of functional recovery was done by Basso, Beattie, and Breshnahan Scoring or BBB Scoring. In an open field, rats were permitted to roam freely. The capacity to lift the tail and trunk and the ability to move the hind limbs were examined and assessed. The BBB score goes from 0 to 21, with 0 representing complete paralysis and 21 indicating typical hind limb mobility.

### 11. Statistical Analysis

GraphPad Prism (GraphPad Software 8.3.0) was used for the statistical analysis. Multiple groups were compared using 1-way analysis of variance (ANOVA). For multiple groups with 2 independent variables, 2-way ANOVA was conducted. A p-value of $< 0.05$ was considered statistically significant. The data are represented as mean ± standard error of the mean.

## RESULTS

### 1. Myricetin Preserves the Integrity of BSCB and Attenuates Inflammation in Acute Phase

To assess the impact of myricetin on reducing vascular permeability, we employed the Evans blue assay to evaluate BSCB integrity. After 24 hours following SCI, rats in both vehicle and treatment cohorts were intravenously administered 0.5 mL of 2% Evans blue solution. Our observations revealed diminished Evans blue dye infiltration in the treatment cohorts compared

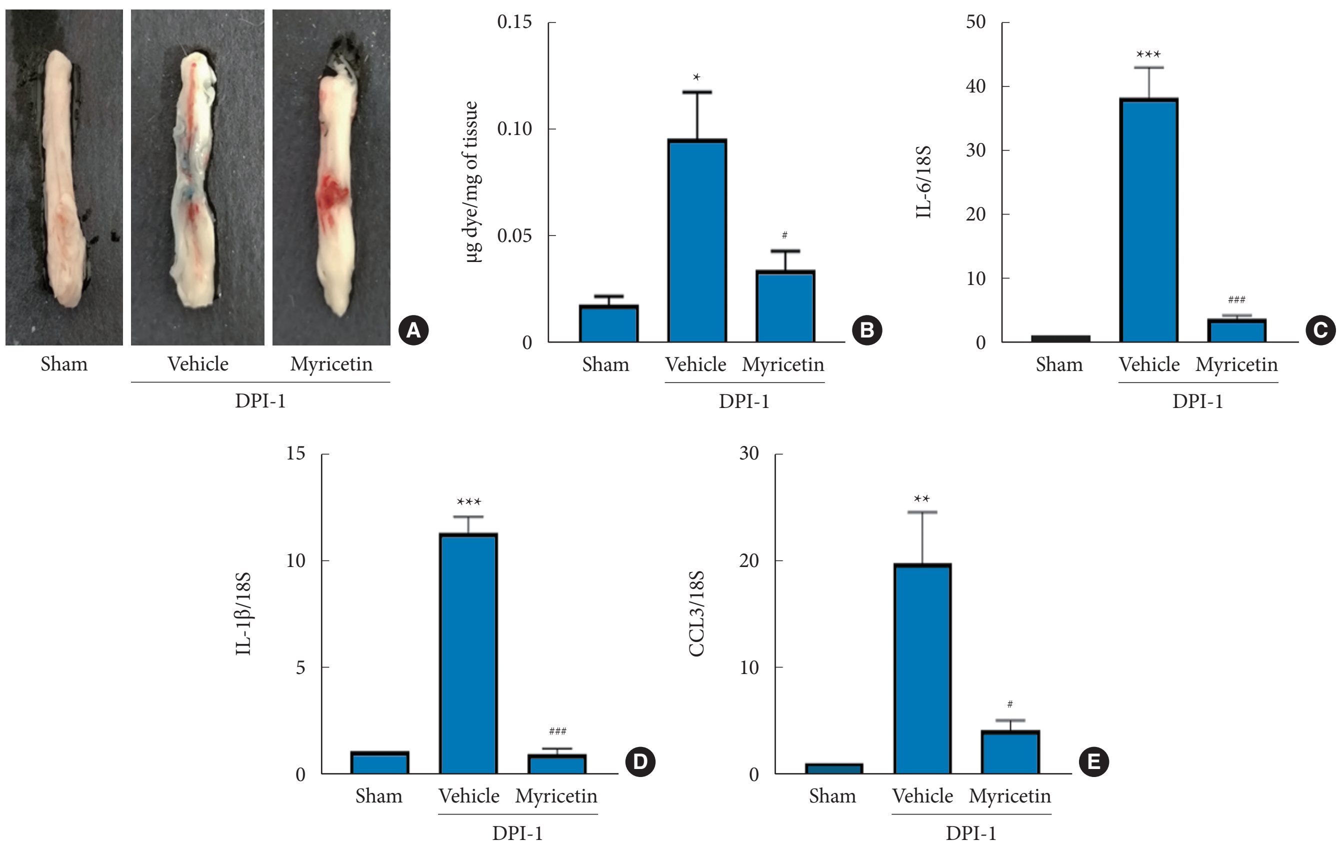


**Fig. 1.** Myricetin improves blood-spinal cord barrier integrity, downregulates the expression of inflammatory markers. (A) Representative spinal cord images at day post injury 1 (DPI-1) for sham, vehicle, and myricetin groups in Evans blue assay. (B) Quantification of Evans blue in the spinal cord tissue sample, performed through spectrophotometric analysis at absorbance wavelength 620 nm. (C) Effect of myricetin on mRNA expressions of interleukin (IL)-6 in sham, vehicle, and myricetin. (D) Effect of myricetin on mRNA expression of IL-1β in sham, vehicle, and myricetin. (E) Effect of myricetin on mRNA expression of CCL3 in sham, vehicle, and treatment. $^{*}p < 0.05$ vs. sham, $^{**}p < 0.01$ vs. sham, $^{***}p < 0.001$ vs. sham, $^{\#}p < 0.05$ vs. vehicle, $^{\#\#\#}p < 0.001$ vs. vehicle (n = 3/group).

to the vehicle cohorts. Notably, the sham group exhibited no Evans blue dye penetration into the spinal cord. Quantitative analysis of homogenized samples from the 3 groups indicated a significant increase in BSCB permeability in the vehicle group (DPI-1), while myricetin-administered groups showed a significant reduction in BSCB permeability and enhanced integrity (Fig. 1A and B).

Recognized for its anti-inflammatory and antioxidant properties, myricetin is pivotal in mitigating the inflammatory response post-SCI. Within the initial 24 hours following injury, neutrophil infiltration ensues, accompanied by an exaggerated release of proinflammatory cytokines detrimental to neurons, ultimately leading to neuronal tissue destruction. This cascade further exacerbates the damage to healthy neuronal tissue. To elucidate myricetin's role in inflammation, we assessed the mRNA expressions of specific proinflammatory cytokines such as IL-6, IL-1β, and chemokines such as CCL3. In the DPI-1 vehicle groups, a significant upsurge in proinflammatory cytokines was evident, contrasted by a marked decrease in the groups treated with a single dose of myricetin (Fig. 1C–E).

**2. LIMK is a Potential Target for Myricetin**

Myricetin was docked against the LIMK protein (PDB id 7B8W) according to the procedure mentioned in the method section. As BMS-5 has been found to be an effective LIMK inhibitor, we docked both BMS-5 (as a standard) and myricetin to evaluate their binding affinities toward the active site of LIMK. We observed that myricetin had a significantly high binding affinity (glide score -12.22 kcal/mol) than the standard BMS-5 (-5.05 kcal/mol) (Fig. 2A and B). This observation indicated that myricetin can bind effectively to the active site of LIMK This effective binding is the first step toward a successful mod-

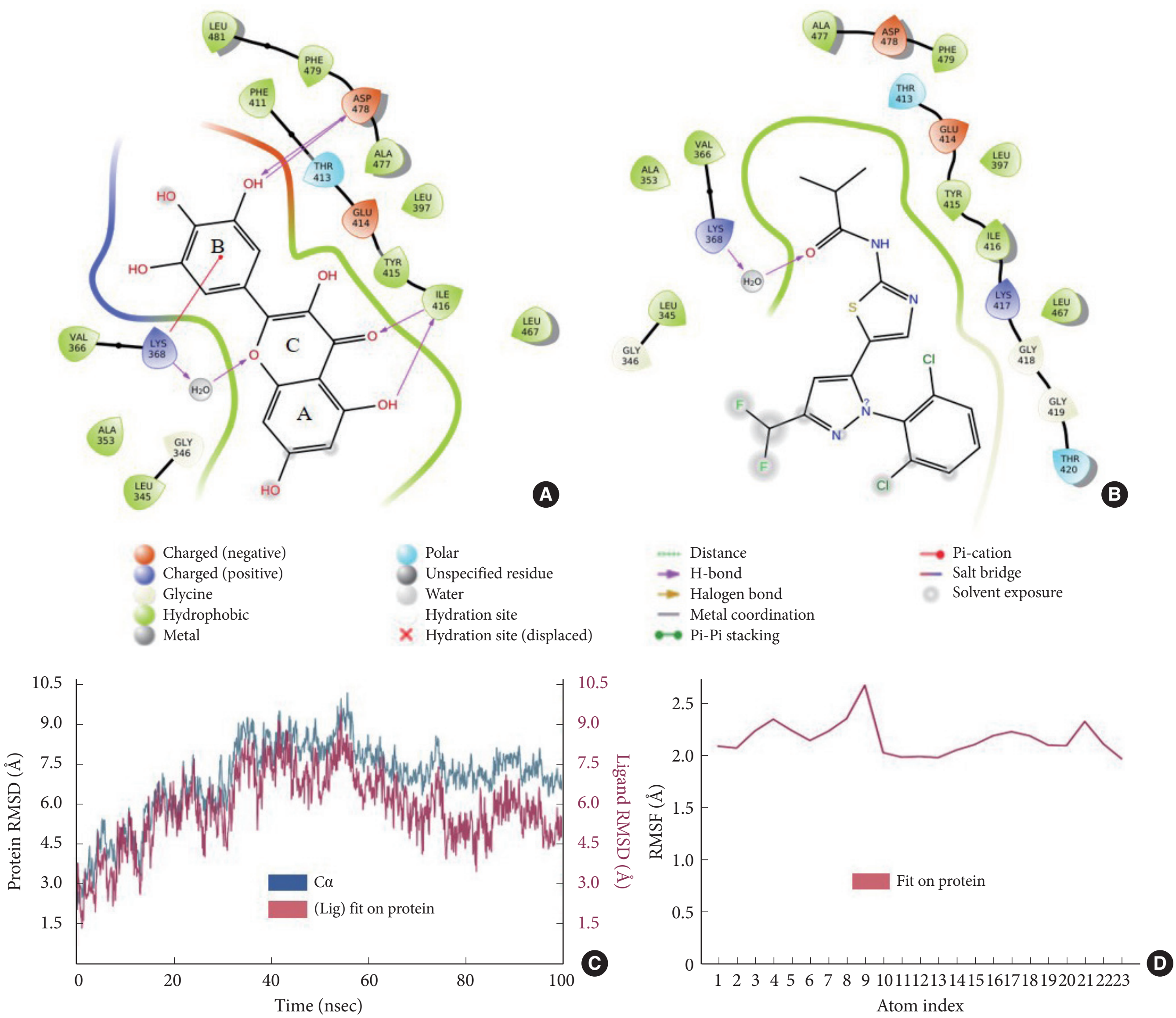


**Fig. 2.** Computational docking model and molecular dynamic simulation study establish LIMK as a potential target for myricetin. (A) Docking of myricetin against LIMK protein (PDB id 7B8W) with a glide score -12.22 kcal/mol. (B) Docking of BMS-5 against LIMK protein (PDB id 7B8W) with a glide score of -5.05 kcal/mol. (C) The root mean square deviation (RMSD) of the holo system (Myricetin-LIMK complex) showed between 3 and 7.5 Å. (D) The root mean squared fluctuation (RMSF) graph of the holo system (myricetin-LIMK complex) exhibited RMSF values ranging from 2 to 2.5 Å. LIMK, Lin-11, Isl-1, and Mec-3 kinase.

ulation of LIMK. If we dig deep into the interactions that occur between myricetin and the protein, we can observe the clear picture. On contrary to a single intermolecular hydrogen bonding between lys 368 and the carbonyl group of the amide functionality resulting in a lower binding affinity for BMS-5, myricetin scores well owing to its interactions namely with ile 416 (hydrogen bonding with the carbonyl of the C ring and the hydroxyl group of the A ring), lys 368 (pi-cation interaction with the phenyl ring B), and asp 478 (hydrogen bonding with one of the 3 hydroxyl groups of the phenyl ring B). These interactions collectively account for a seamless binding affinity of myricetin toward LIMK.

To investigate the molecular mechanisms involved in myricetin binding to the active site of LIMK, a 100-ns molecular dynamic simulation was performed (PDB id 7B8W). The RMSD of the holo system (myricetin-LIMK complex) was between 3 and 7.5 Å (Fig. 2C). The lower RMSD value and amplitude is indicative of better stabilization of LIMK when myricetin is

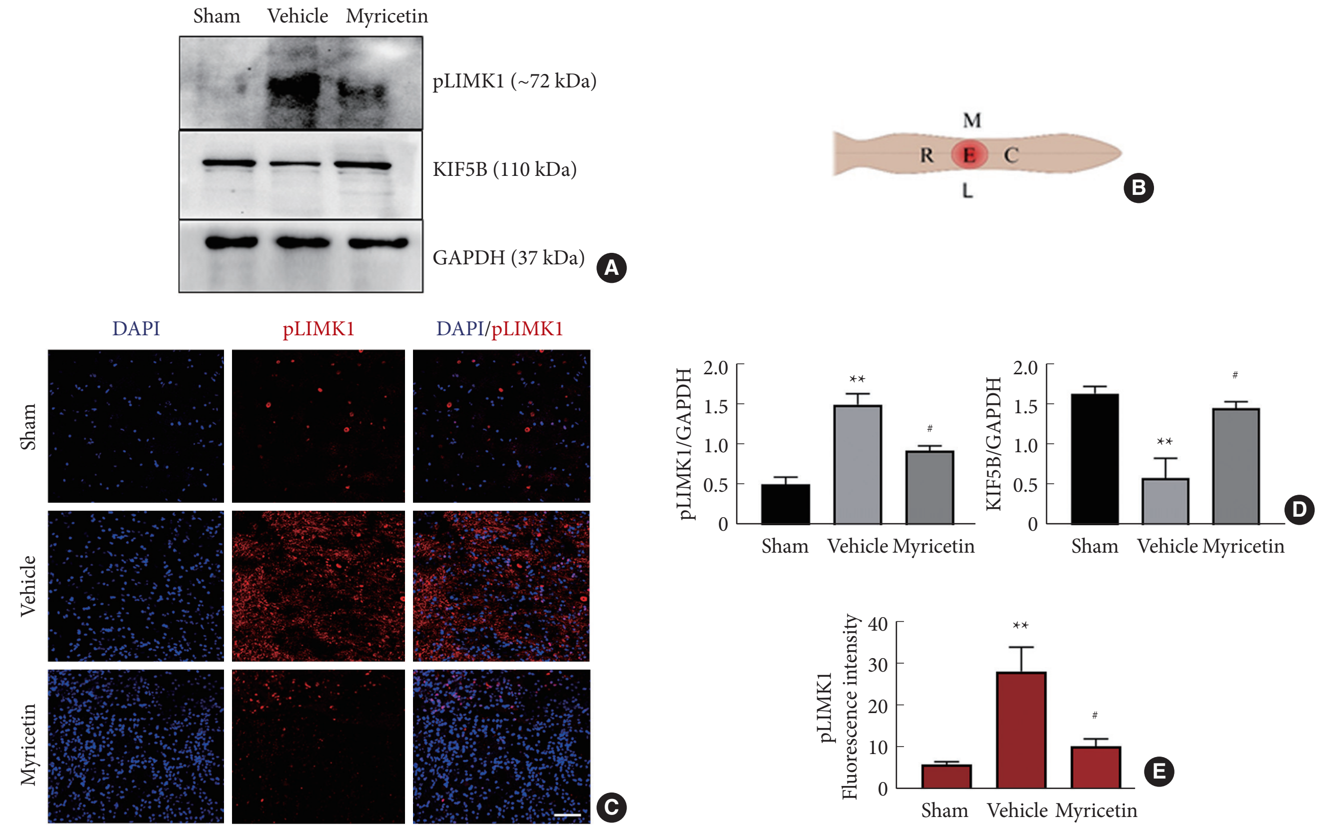


Fig. 3. Myricetin reduces LIMK expression at chronic phase and stabilizes microtubules. (A) Representative Western blot images of phosphorylated LIMK, KIF5B, and GAPDH for sham, vehicle and myricetin in spinal cord tissue. (B) The reference axis showing rostral (R), caudal (C), epicenter (E), medial (M), and lateral (L) regions in the longitudinal image of the injured spinal cord. The epicenter region is further analyzed in panel C by immunohistochemistry. (C) Representative immunohistochemistry images of phosphorylated LIMK for sham, vehicle and myricetin in spinal cord tissue ($n = 3$/group) (scale bar, 50 μm). (D) Quantification of phosphorylated LIMK1, and KIF5B respectively. (E) Fluorescence intensity quantification of phosphorylated LIMK1. Data is represented as mean ± standard error of the mean ($n = 3$). DAPI, 4´6-diamidino-2-phenylindole; LIMK, Lin-11, Isl-1, and Mec-3 kinase. $^{**}p < 0.01$ vs. sham, and $^{\#}p < 0.05$ vs. vehicle.

present as a ligand. The stabilization effect was visible from the 60-ns timeframe. The root mean squared fluctuation (RMSF) graph of the holo system (myricetin-LIMK complex) exhibited RMSF values ranging from 2 to 2.5 Å (Fig. 2D). This cumulative RMSD and RMSF values indicate that myricetin has the ability to bind effectively to LIMK active site and stabilize the protein. Further studies explained later shall enlighten about the modulation of LIMK by myricetin at the molecular level.

### 3. Myricetin Downregulates the Expression of LIMK at Chronic Phase and Stabilizes Microtubules

In our previous study, we found the most significant upregulation of phosphorylated LIMK1 at DPI-28. So, we decided to check the expression of LIMK after myricetin treatment at this particular time point. Myricetin treatment was found to be effective in significantly downregulating the expression of phosphorylated LIMK1 compared to the vehicle group (Fig. 3A and D). Upon assessing the impact on the microtubule-specific marker, we observed a notable increase in KIF5B expression when treated with myricetin compared to the vehicle (Fig. 3A and D). In addition to Western blot analysis, we validated this observation using immunohistochemistry. Furthermore, we identified a significant elevation in phosphorylated LIMK1 levels in the vehicle group compared to the sham group. Conversely, the myricetin-treated group exhibited a marked decrease in phosphorylated LIMK1 levels compared to the vehicle group (Fig. 3C and E).

### 4. LIMK Inhibition With Myricetin Attenuates Glial Scar Formation and Enhances Neuroprotection

Glial scar or astrocytic scar, after extensive inflammation and tissue damage, is one of the typical characteristics of the chronic

 https://doi.org/10.14245/ns.2448546.273

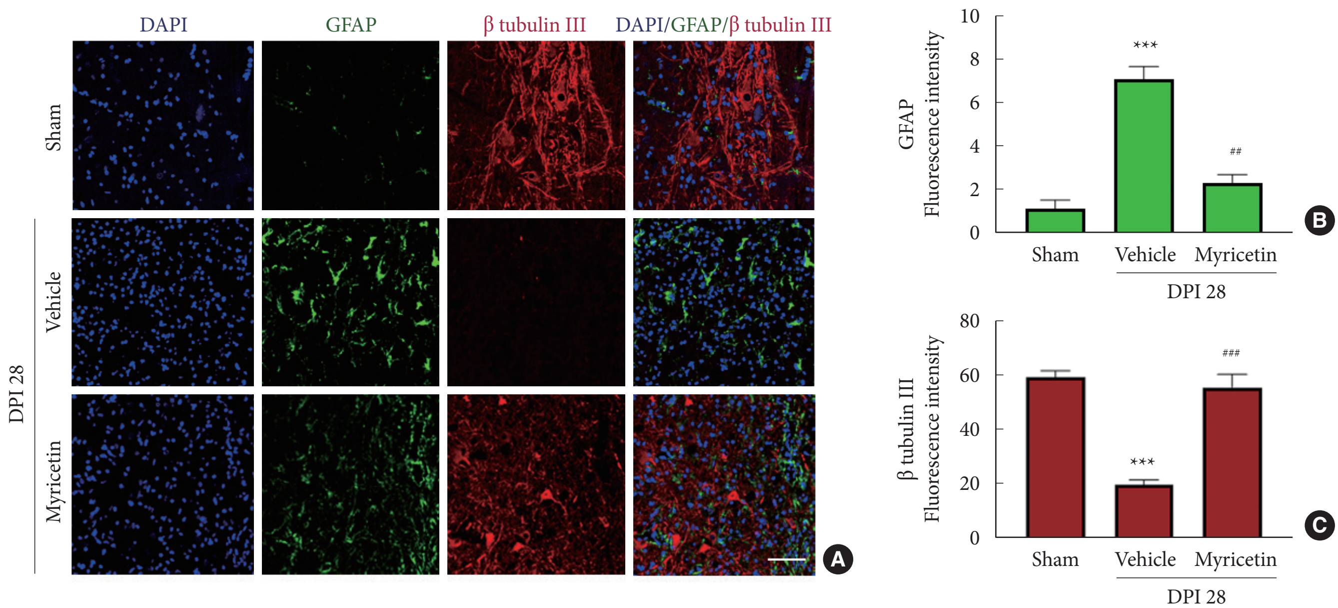


**Fig. 4.** Inhibition of LIMK modulates the expressions of glial fibrillary acidic protein (GFAP), and β tubulin III. (A) Representative immunohistochemistry images of GFAP, and β tubulin III for sham, vehicle, and myricetin in spinal cord tissue (n = 3/group) (scale bar, 50 μm). (B, C) Fluorescence intensity quantification of GFAP, and β tubulin III, respectively. Data is represented as mean ± standard error of the mean. DAPI, 4´6-diamidino-2-phenylindole; DPI, day post injury. $^{***}p < 0.001$ vs. sham, $^{\#\#\#}p < 0.001$ vs. vehicle, $^{\#\#}p < 0.01$ vs. vehicle.

phase in SCI. Gliosis is the reactive cellular mechanism that is aided by astrocytes.[20] Astrocytes are one of the important components of the CNS; however, they take a different turn when an injury or insult occurs in the CNS. Glial fibrillary acidic protein (GFAP) is an intermediate filament protein expressed mainly in astrocytes. As observed in Fig. 4A and B, the enhanced expression of GFAP is significant in vehicle groups (DPI-28), as compared to sham groups. There has been a significant reduction in the expression of this marker in the case of myricetin-treated groups compared to vehicle group.

Class III β-tubulin is one of the essential components of the neuronal cytoskeleton and is expressed only in neuronal cells but not in glial cells.[21] The injury-related alterations in the cytoskeleton are visible in Fig. 4A and C, indicating neuronal loss in the DPI-28 vehicle groups as compared to the sham group. When myricetin-treated groups are considered, a significant change is observed compared to vehicle groups.

### 5. Myricetin Modulates Fibrotic Scar Formation and Improves Functional Recovery After SCI

In SCI, extracellular matrix (ECM) remodeling is observed extensively. The fibrotic scar is a major condition observed in chronic phases that inhibits neuronal regeneration.[22] ECM remodeling is one of the vital conditions that SCI accompanies due to the deposition of laminin. The main source of laminin is the endothelial progenitor cells, which actively modulate the secretion of this growth regulator. The expression of laminin is known to affect the production of the basement membrane. They participate in forming the glial scar.[23] In the chronic phase, after administering myricetin for 7 days, the expression of laminin was modulated. From Fig. 5A and B, there is a clear indication of fibrotic scar formation at DPI-28 in vehicle group. The results implicate that after almost one month of injury, the reactive astrocytes, as well as the neurons of the lesioned site, expressed laminin; however, in the myricetin-treated group, the expression of laminin was modulated, suggesting that there was an alteration in fibrous tissue formation favoring neurite outgrowth. After injury in the lower thoracic region in the spinal cord, paraplegia was observed which was confirmed by BBB scoring. Visually observing the motor coordination, the rats were given a score according to a pre-defined criterion. The score advanced eventually in myricetin-treated group with day points when compared with the vehicle group (Fig. 5C).

## DISCUSSION

The current landscape of therapeutic strategies for SCI remains contentious, with ongoing research summarizing various ap-

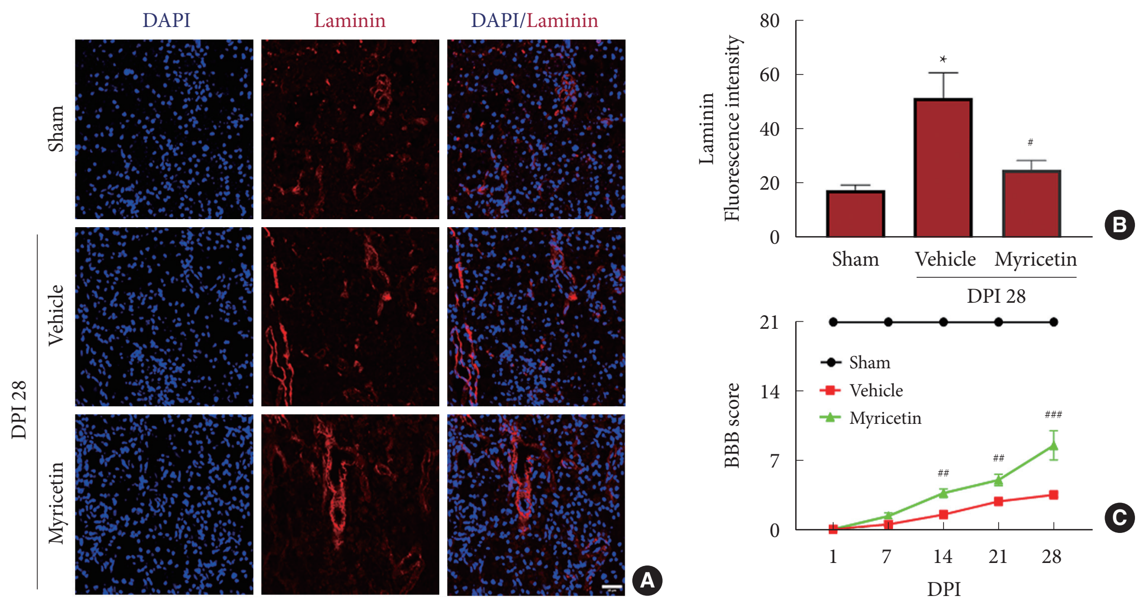


**Fig. 5.** Inhibition of LIMK through Myricetin modulates the expressions of laminin and promotes neuroprotection through functional recovery. (A) Representative immunohistochemistry images of laminin for sham, vehicle, and myricetin in spinal cord tissue (2–3 fields/slide, n = 3/group) (scale bar, 50 μm). (B) Fluorescence intensity quantification of laminin. (C) Functional recovery was assessed in open-field testing by using the 21-point Basso, Beattie, and Bresnahan (BBB) locomotor test at 1, 7, 14, 21, and 28 days after SCI (n = 6/group). Data is represented as mean ± standard error of the mean. DAPI, 4′6-diamidino-2-phenylindole; DPI, day post injury. $^{*}p < 0.05$ vs. sham, $^{###}p < .001$ vs. vehicle, $^{##}p < 0.01$ vs. vehicle, and $^{#}p < 0.05$ vs. vehicle.

proaches at different levels of SCI.[24] To date, Methylprednisolone stands as the sole Food and Drug Administration-approved treatment for reducing inflammatory conditions and oxidative stress.[25] However, its limitations, including various side effects and its role limited to symptomatic relief, persist.[26]

Despite the existence of multimodal treatment strategies encompassing invasive procedures such as surgeries, mesenchymal stem cell transplantations, immunotherapy, implants, light-based therapies, and herbal-derived drugs, significant challenges remain.[27,28] Emerging treatment modalities aim to develop novel delivery systems and therapeutic strategies targeting inflammatory and apoptotic cascades, along with molecular pathways, to enhance behavioral aspects related to mobility and locomotion.[29,30]

LIMKs, downstream effectors of small G proteins within the Rho GTPases superfamily, regulate various cellular processes crucial for neural function. Studies have implicated LIMK in processes like cell motility, morphogenesis, differentiation, and apoptosis, highlighting its potential significance in pathologies like metastasis.[7,31,32] Besides this, LIMKs were found to play a crucial role in central sensitization and chronic pain development, suggesting new therapeutic targets for clinical treatment. In both spared nerve injury and post-surgical pain animal models, administering a particular LIMK inhibitor, intrathecally, during the activation phase of LIMK significantly alleviated central sensitization and suppressed the development of pain behaviors.[33] Targeting LIMKs explicitly may help prevent side effects caused by the uncontrollably involvement of other kinases, as they are downstream of the pathway involving cofilin, their principal substrate that has been identified.[34] Notably, our previous research identified elevated levels of LIMK and its downstream effector cofilin post-SCI, suggesting a novel therapeutic approach.[11]

Myricetin, a flavonoid compound abundant in various food sources, exhibits anti-inflammatory and neuroprotective properties.[35] Its ability to mitigate oxidative stress and inflammation, along with its polyphenolic nature facilitating binding to different kinases, makes it a promising candidate for various ailments, including neurodegenerative disorders.[36] It is pertinent to mention that polyphenols are generally regarded as fountains of health. Compared to other flavonoids, myricetin has a higher level of antioxidant activity because its pyrogallol ring B has 3 hydroxyl groups. Studies conducted *in vitro* have shown that the 2 hydroxyl groups and the double-bonded oxygen group of myricetin are responsible for the mineral chelation. Hence, in addition to eliminating the reactive oxygen species (ROS), myric-


https://doi.org/10.14245/ns.2448546.273

etin also chelates intracellular transition metal ions exhibiting antioxidant activity. The catechol groups in myricetin's structure, which result in semi-quinone radicals, are responsible for its pro-oxidative effect. Since oxidative stress is one of the primary causes of inflammation, anti-inflammatory and antioxidant properties are closely related.[37,38] Given the exacerbating role of LIMK pathway activation in SCI pathophysiology, targeting this pathway with myricetin may emerge as a potential therapeutic strategy.[11]

In our study, we administered myricetin post-SCI to inhibit early-stage inflammation and continued oral administration to evaluate its effects in chronic phases. Preliminary docking studies revealed myricetin's potential to bind with LIMK with favorable interaction profile. Though drug binding assay is a common method to measure whether 2 molecules interact with each other, it has certain limitations. The kind of drug being measured—whether it is "free," "total," or "bound"—requires more attention. Since it might be challenging to quantify these fractions to an exact amount, it's critical to carefully plan and define the experiment. It's important to comprehend how the analytical approach eventually impacts the *in vivo* equilibrium since it could not be an accurate depiction of that environment.[39] Specifically, a great deal of experimentation fails to quantify the reactants' affinity for each other. On the contrary, the docking techniques employed in structure-based virtual screening make it possible to predict a ligand's affinity and mechanism of binding for the target protein receptor in a fast and affordable manner. Advancements in computational technology have led to more practical uses for molecular models, including improved approximations with respect to accuracy and computational efficiency.[40] In addition to docking studies, we performed molecular dynamics simulation studies to gain insight into the behavior of an actual physical system or process. The myricetin-LIMK complex's low RMSF values suggest that the target molecule does not deviate much from the average position, revealing that they are more rigid throughout the simulation. Simultaneously, the smaller RMSD value indicates more similarity between the 2 structures.

In a previous study by Huang et al., myricetin administration at a dose of 10 mg/kg/day suppressed the activation of microglia, downregulated the expression of proinflammatory mediators and prevented the loss of dopaminergic neurons in a lipopolysaccharide induced model of Parkinson's disease.[41] Myricetin administered orally once daily at a dose of 10 or 20 mg/kg has been demonstrated to ameliorate neurological deficits and lessen neuronal apoptosis and infarct area in a rat model of middle cerebral artery occlusion by suppressing abnormally increased ROS as well as enhancing abnormally decreased levels of reduced glutathione, superoxide dismutase activity, and mitochondrial membrane potential in ischemic brain tissues.[17] In a rat model of Alzheimer's disease caused by streptozotocin, administering myricetin (5 or 10 mg/kg, i.p., starting 1 day before stereotactic surgery and lasting 21 days) was shown to reduce memory impairment.[42] Based on these findings, we evaluated the effects of myricetin in the chronic phase of SCI by administering it orally for continuous 7 days at a dose of 10 mg/kg/day. The distribution and metabolism of myricetin after oral administration has already been characterized. Using ultraperformance liquid chromatography–tandem mass spectrometry, Dang et al.[43] investigated the pharmacokinetic characteristics of myricetin. Myricetin was administered to rats intravenously and orally, and its bioavailability in plasma was subsequently analyzed. *In vivo*, myricetin was absorbed by passive diffusion, as shown by a dose-dependent rise in maximum concentrations (Cmax) and area under curve following oral administration. Myricetin was slowly absorbed due to its low aqueous solubility, as observed by the comparatively long Tmax (6.4 hours) to reach Cmax ($1,488.75 \pm 200.78$ ng/mL). Substances that being a small molecule, having a molecular weight of less than 500 and a LogP of around 2–4 are often able to pass across the blood-brain barrier (BBB). Notably, myricetin has a molecular weight of 318.237 and a reported LogP value of 2.76. Hence, it is assumed that myricetin can penetrate the BBB and show neuroprotective effects in the CNS. A metabolic hypothesis also suggests that the myricetin taken orally might be transformed into a metabolite (3, 5-dihydroxyphenylacetic acid) that crosses the BBB and exerts neuroprotective effects.[36] In our study, myricetin-treated groups at DPI-28, showed a substantial downregulation in the expression of phosphorylated (active) LIMK in conjunction with microtubule stability. Furthermore, myricetin treatment demonstrated efficacy through fostering neuroprotection, reducing glial and modulating fibrotic scar formation, and improving motor function recovery, as evidenced by the behavioral data.

## CONCLUSION

Overall our results demonstrate that LIMK can be a potential target for myricetin with favorable interaction profile. Hence, targeting LIMK with myricetin may serve as an adjunctive therapy in SCI management, offering a promising nutraceutical approach.

## NOTES

**Conflict of Interest:** The authors have nothing to disclose.

**Funding/Support:** This study received no specific grant from any funding agency in the public, commercial, or not-for-profit sectors.

**Acknowledgments:** Authors would like to thank Department of Pharmaceuticals, Ministry of Chemicals and Fertilizers, Govt. of India and NIPER Ahmedabad. The authors gratefully acknowledge the funding assistance provided by Department of Biotechnology, Govt. of India, New Delhi for the grant no. BT/PR47609/CMD/150/19/2023.

**Author Contribution:** Conceptualization: HK; Formal analysis: AR, SS; Methodology: AR, SS, RD; Project administration: HK; Visualization: HK; Writing – original draft: AR, SS, RD; Writing – review & editing: AS.

**ORCID**

Abhishek Roy: 0000-0003-4081-1054
Santimoy Sen: 0000-0001-9788-7493
Rudradip Das: 0000-0002-1303-9997
Amit Shard: 0000-0003-4109-6275
Hemant Kumar: 0000-0002-6434-0245

## REFERENCES

1. Alizadeh A, Dyck SM, Karimi-Abdolrezaee S. Traumatic spinal cord injury: an overview of pathophysiology, models and acute injury mechanisms. Front Neurol 2019;10:282.
2. Yao X. The role of GABA in spinal cord injury. Neurospine 2022;19:669-70.
3. Yiu G, He Z. Glial inhibition of CNS axon regeneration. Nat Rev Neurosci 2006;7:617-27.
4. Fujita Y, Yamashita T. Axon growth inhibition by RhoA/ROCK in the central nervous system. Front Neurosci 2014;8:338.
5. Dickson BJ. Rho GTPases in growth cone guidance. Curr Opin Neurobiol 2001;11:103-10.
6. Luo L. Rho GTPases in neuronal morphogenesis. Nat Rev Neurosci 2000;1:173-80.
7. Manetti F. Recent findings confirm LIM domain kinases as emerging target candidates for cancer therapy. Curr Cancer Drug Targets 2012;12:543-60.
8. Prunier C, Prudent R, Kapur R, et al. LIM kinases: cofilin and beyond. Oncotarget 2017;8:41749-63.
9. Manetti F. Recent advances in the rational design and development of LIM kinase inhibitors are not enough to enter clinical trials. Eur J Med Chem 2018;155:445-58.
10. Li Y, Hu F, Chen HJ, et al. LIMK-dependent actin polymerization in primary sensory neurons promotes the development of inflammatory heat hyperalgesia in rats. Sci Signal 2014;7:ra61.
11. Roy A, Pathak Z, Kumar H. Investigating LIM (Lin-11, Isl-1, and Mec-3) kinases and their correlation with pathological events and microtubule dynamics in an experimental model of spinal cord injury in rats. ACS Pharmacol Transl Sci 2024;7:667-79.
12. Ullah A, Munir S, Badshah SL, et al. Important flavonoids and their role as a therapeutic agent. Molecules 2020;25:5243.
13. Maggiolini M, Recchia AG, Bonofiglio D, et al. The red wine phenolics piceatannol and myricetin act as agonists for estrogen receptor alpha in human breast cancer cells. J Mol Endocrinol 2005;35:269-81.
14. Wang G, Wang JJ, Tang XJ, et al. In vitro and in vivo evaluation of functionalized chitosan-Pluronic micelles loaded with myricetin on glioblastoma cancer. Nanomedicine 2016;12:1263-78.
15. Ko SY. Myricetin suppresses LPS-induced MMP expression in human gingival fibroblasts and inhibits osteoclastogenesis by downregulating NFATc1 in RANKL-induced RAW 264.7 cells. Arch Oral Biol 2012;57:1623-32.
16. Wang C, Ouyang S, Zhu X, et al. Myricetin suppresses traumatic brain injury-induced inflammatory response via EGFR/AKT/STAT pathway. Sci Rep 2023;13:22764.
17. Wu S, Yue Y, Peng A, et al. Myricetin ameliorates brain injury and neurological deficits via Nrf2 activation after experimental stroke in middle-aged rats. Food Funct 2016;7:2624-34.
18. Friesner RA, Banks JL, Murphy RB, et al. Glide: a new approach for rapid, accurate docking and scoring. 1. Method and assessment of docking accuracy. J Med Chem 2004;47:1739-49.
19. Wang H, Fan X, Xie PP, et al. Deciphering the diversified metabolic behavior of hydroxyalkyl ferrocidiphenols as anticancer complexes. J Med Chem 2024;67:1209-24.
20. Bradbury EJ, Burnside ER. Moving beyond the glial scar for spinal cord repair. Nat Commun 2019;10:3879.
21. Katsetos CD, Herman MM, Mörk SJ. Class III beta-tubulin in human development and cancer. Cell Motil Cytoskeleton 2003;55:77-96.
22. Li Z, Yu S, Hu X, et al. Fibrotic scar after spinal cord injury: crosstalk with other cells, cellular origin, function, and mech-

 https://doi.org/10.14245/ns.2448546.273

anism. Front Cell Neurosci 2021;15:720938.
23. Ayazi M, Zivkovic S, Hammel G, et al. Fibrotic scar in CNS injuries: from the cellular origins of fibroblasts to the molecular processes of fibrotic scar formation. Cells 2022;11:2371.
24. Dolma S, Adhikari K, Mamidi T, et al. Ethamsylate attenuates mutilated secondary pathogenesis and exhibits a neuroprotective role in experimental model of spinal cord injury. Neuroscience 2022;484:26-37.
25. Cheung V, Hoshide R, Bansal V, et al. Methylprednisolone in the management of spinal cord injuries: lessons from randomized, controlled trials. Surg Neurol Int 2015;6:142.
26. Lewis NE, Tabarestani TQ, Cellini BR, et al. Effect of acute physical interventions on pathophysiology and recovery after spinal cord injury: a comprehensive review of the literature. Neurospine 2022;19:671-86.
27. Ma YH, Liang QY, Ding Y, et al. Multimodal repair of spinal cord injury with mesenchymal stem cells. Neurospine 2022; 19:616-29.
28. Lee S, Cho DC, Han I, et al. Curcumin as a promising neuroprotective agent for the treatment of spinal cord injury: a review of the literature. Neurospine 2022;19:249-61.
29. Gadot R, Smith DN, Prablek M, et al. Established and emerging therapies in acute spinal cord injury. Neurospine 2022; 19:283-96.
30. Jarrah R, Sammak SE, Onyedimma C, et al. The role of alginate hydrogels as a potential treatment modality for spinal cord injury: a comprehensive review of the literature. Neurospine 2022;19:272-80.
31. Mali RS, Kapur R. Targeting Rho associated kinases in leukemia and myeloproliferative neoplasms. Oncotarget 2012; 3:909-10.
32. Rath N, Olson MF. Rho-associated kinases in tumorigenesis: re-considering ROCK inhibition for cancer therapy. EMBO Rep 2012;13:900-8.
33. Yang X, He G, Zhang X, et al. Transient inhibition of LIMKs significantly attenuated central sensitization and delayed the development of chronic pain. Neuropharmacology 2017;125: 284-94.
34. Berabez R, Routier S, Bénédetti H, et al. LIM kinases, promising but reluctant therapeutic targets: chemistry and preclinical validation in vivo. Cells 2022;11:2090.
35. Semwal DK, Semwal RB, Combrinck S, et al. Myricetin: a dietary molecule with diverse biological activities. Nutrients 2016;8:90.
36. Li J, Xiang H, Huang C, et al. Pharmacological actions of myricetin in the nervous system: a comprehensive review of preclinical studies in animals and cell models. Front Pharmacol 2021;12:797298.
37. Imran M, Saeed F, Hussain G, et al. Myricetin: a comprehensive review on its biological potentials. Food Sci Nutr 2021; 9:5854-68.
38. Gupta G, Siddiqui MA, Khan MM, et al. Current pharmacological trends on myricetin. Drug Res (Stuttg) 2020;70: 448-54.
39. Mayer AP, Hottenstein CS. Ligand-binding assay development: what do you want to measure versus what you are measuring? AAPS J 2016;18:287-9.
40. Grinter SZ, Zou X. Challenges, applications, and recent advances of protein-ligand docking in structure-based drug design. Molecules 2014;19:10150-76.
41. Huang B, Liu J, Ma D, et al. Myricetin prevents dopaminergic neurons from undergoing neuroinflammation-mediated degeneration in a lipopolysaccharide-induced Parkinson's disease model. J Funct Foods 2018;45:452-61.
42. Ramezani M, Darbandi N, Khodagholi F, et al. Myricetin protects hippocampal CA3 pyramidal neurons and improves learning and memory impairments in rats with Alzheimer's disease. Neural Regen Res 2016;11:1976-80.
43. Dang Y, Lin G, Xie Y, et al. Quantitative determination of myricetin in rat plasma by ultra performance liquid chromatography tandem mass spectrometry and its absolute bioavailability. Drug Res (Stuttg) 2014;64:516-22.